*Research supported in part by Union Carbide Corp. and by Oak Ridge Associated Universities under contract with the U. S. Atomic Energy Commission, and in part by the U. S. Office of Naval Research.

†Present address: Department of Physics, Kansas State University, Manhattan, Kan.

[1]I. A. Sellin, D. J. Pegg, M. Brown, W. W. Smith, and B. Donnally, Phys. Rev. Letters 27, 1108 (1971).

[2]This multiplet is of considerable importance in the ion He^-, where it is the ground state. The lifetime of the $J=\frac{5}{2}$ level has been measured recently [L. M. Blau, R. Novick, and D. Weinflash, Phys. Rev. Letters 24, 1268 (1970)].

[3]B. Donnally, W. W. Smith, D. J. Pegg, M. Brown, and I. A. Sellin, Phys. Rev. A 4, 122 (1971).

[4]L. C. Northcliffe, in *Annual Reviews of Nuclear Science*, edited by E. Segrè (Annual Reviews, Palo Alto, Calif., 1963), Vol. 13, p. 83.

[5]H. D. Betz, Phys. Rev. Letters 25, 211 (1970); 25, 903 (1970).

[6]W. W. Smith, Bailey Donnally, D. J. Pegg, M. Brown, and I. A. Sellin, in *Abstracts of the Seventh International Conference on the Physics of Electronic and Atomic Collisions* (North-Holland, Amsterdam, 1971), p. 513.

[7]I. S. Dmitriev, Y. A. Teplova, and V. S. Nikolaev, Zh. Eksperim. i Teor. Fiz. 61, 1359 (1971) [Sov. Phys. JETP 34, 723 (1972)].

[8]E. Hubbard and E. Lauer, Phys. Rev. 98, 1814 (1955); R. A. Brown and G. D. Simons, Nucl. Instr. Methods 58, 274 (1968). These references indicate that, in the energy range being considered, 5 $\mu g/cm^2$ of carbon is sufficient to establish charge-state equilibrium for incident oxygen ions.

[9]We have not measured this. The multiplier used was manufactured by Mullard. The very similar Bendix Channeltron cone-input unit has an efficiency of 98% for electrons of a few hundred electron volts according to the manufacturer.

[10]I. A. Sellin and D. Pegg (unpublished).

[11]J. B. Marion and F. C. Young, *Nuclear Reaction Analysis* (North-Holland, Amsterdam, 1968).

[12]The charge-state fractions ϕ_i do have a dependence on target material that may be significant in some applications. There is also considerable systematic variation in the values for the same projectile-target combinations among the results of different investigators. Results for oxygen ions on carbon, gold, nickel, and other materials are given by D. Bernard, B. Bonner, G. Phillips, and P. Stelson [Nucl. Phys. 73, 513 (1965)] and W. Booth and I. Grant [Nucl. Phys. 63, 481 (1965)]. The second paper discusses possible reasons for this dependence on target material.

[13]These data have not been corrected for possible small normalization errors due to straggling and also to the dependence of multiple beam scattering on foil thickness. It seems to us premature to speculate on the reason for this apparent dependence of Y on target material. We merely note that the yield appears to have a broad maximum near $Z_{target}=13$. The effect of foil-surface conditions in determining the yield is basically unknown. It is known, at least in the case of carbon foils, that they become thicker with time of exposure to the beam, possibly because of deposition of carbon from "cracked" pump oil in the vacuum system. This phenomenon has no appreciable effect on the yield.

[14]Using a value of 25 nsec for the $J=\frac{5}{2}$ state lifetime will raise the values of Ref. 7 relative to this work.

[15]For a background discussion of the expressions for the capture cross section obtained by N. Bohr and by H. Brinkman and H. Kramers, see the article by H. Bethe and J. Ashkin, in *Experimental Nuclear Physics*, edited by E. Segrè (Wiley, New York, 1953), Vol. 1, p. 191.

[16]N. Bohr and J. Lindhard, Dan. Mat. Fys. Medd. 28, No. 7 (1954). Experimental evidence for the decrease in the capture cross section with excitation is given (for Cl ions in low-density gases) by G. Ryding, H. D. Betz, and A. Wittkower [Phys. Rev. Letters 24, 123 (1970)]. It may be that this effect is somewhat suppressed in solids, but partial suppression will not invalidate the qualitative argument we are making.

PHYSICAL REVIEW A VOLUME 7, NUMBER 2 FEBRUARY 1973

Transition Probabilities and Multiple Ionizations of Ions by High-Energy-Electron Impact*

Yukap Hahn† and Kenneth M. Watson
Physics Department and Lawrence Berkeley Laboratory, University of California, Berkeley, California 94720

(Received 2 August 1972)

The single-particle model for atoms and ions is used to calculate the transition probabilities to bound and continuum electronic states. The projection operators in the semiclassical approximation derived previously are applied to treat the large numbers of final states involved. Ionization cross sections of atoms and ions by high-energy-electron impact are then estimated. The ionization cross sections result both from direct transition to the continuum and from inelastic scattering followed by Auger emission.

I. INTRODUCTION

Electron impact provides a possible mechanism for production of highly ionized beams to be used for injection into heavy-ion accelerators. With most of the Periodic Table and as many as twenty to thirty steps of ionization considered of interest, it is evident that several thousand ionization cross

sections may be required to estimate ionization rates. It is also evident that great accuracy is not feasible in the calculation of so many cross sections. The purpose of this paper is to obtain a reasonable estimate in parametrized form for the many required cross sections.

We shall assume the bombarding electrons to have energies large compared with the relevant electronic ionization potentials. Two mechanisms for ionization will be considered: (a) direct transitions to continuum states; (b) excitations of inner-shell electrons to excited states followed by Auger emission. Several studies of the fluorescence yield[1-3] indicate that process (b) is no less important than (a) for producing ionization.

To obtain a quantitative estimate of the contribution from the processes (a) and (b), it is desirable first to evaluate the transition probabilities of both inner- and outer-shell electrons to various allowed excited states, including the continuum. For the target atoms and ions, we choose a simple single-particle model. Based on the extensive studies carried out earlier using the Hartree–Fock[4] and Fermi–Thomas models,[5] Green *et al.*[6] have derived an even simpler model for complex atoms, with analytic potentials of the Coulombic plus Wood–Saxon type. Although rather crude in the prediction of term values, this model is probably sufficient for our present purpose. The form of the potential we have adopted contains essentially one adjustable parameter d for each core charge Z_C.

The transition probabilities to a group of excited states and the continuum may be conveniently evaluated using the projection operators derived earlier[7] in the semiclassical approximation. Since the model potential we have chosen is local and in a single-particle form, very little modification is necessary; we have used the simple form Λ^l_{B0} in the notation of Ref. 7.

In Sec. II we define the model potential for the target ions. Since we present the result of our calculations at only several typical values of Z_C and the degree Z_I of ionization, the intermediate steps involved in the energy eigenvalue calculations and scaling should be helpful in obtaining results at other values of Z_C and Z_I. We give a brief discussion of this in Appendix A. The transition probabilities with dipole coupling are defined in terms of the semiclassical projection operators, and the complete set of transitions allowed by the selection rules and exclusion principle is studied.

The result of Sec. II is then used in Sec. III to estimate the ionization cross sections of ions and atoms by high-energy-electron impact. Contributions from the different competing processes mentioned above are evaluated. With the various simplifying approximations which are expected to be valid for high-energy collisions, the transition probabilities evaluated in Sec. II can be directly related to the ionization cross sections.

II. SINGLE-PARTICLE MODEL AND TRANSITION PROBABILITIES

For simplicity, we adopt the single-particle potential for atoms and ions obtained by Green *et al.*,[6] which was derived by fitting the Hartree–Fock (HF) and Hartree–Fock–Slater (HFS) solutions. Its form is

$$V(r) = (1/r)\,[(Z_C - Z_I - 1)\,Y(r) - Z_C]\,, \tag{2.1}$$

where Z_C is the bare-core nuclear charge of an atom or ion, Z_I is the degree of ionization of the target before the collision ($Z_I = 0$ for a neutral atom), and

$$Y(r) = 1 - \Omega(r)\,, \tag{2.2}$$

where

$$\Omega(r) = [H(e^{r/d} - 1) + 1]^{-1}\,,$$

$$H = \alpha\,(Z_C - Z_I - 1)^{\nu}\,d\,,$$

with

$$\nu = 0.4\,, \quad \alpha = 1.00\,, \quad m = \hbar = e^2 = 1$$

for all Z_C and Z_I. Thus, the only parameter which is varied as a function of Z_C is d, which is assigned the values[6] given in Table I. (We take Green's values.)

The result of the calculation of the single-particle energies E_{nl} is summarized in Tables II–IV for the values $Z_C = 10, 20, \ldots, 80$. For each Z_C, all values of Z_I which correspond to the filled subshells are considered.

As $V(r)$ of (2.1) is Coulombic for large values of r, we expect to have an infinite number of bound states near each ionization threshold. Therefore, the excitation probabilities to these discrete and also to continuum states may be evaluated most conveniently using projection operators. We have shown[7] previously that the projection onto all the bound states generated by the potential $V(r)$ may be given in a semiclassical approximation by

TABLE I. The parameter d (in atomic units) in the single-particle potential as given in Ref. 6. The same values are used for all Z_I at each Z_C.

Z_C	d
10	0.500
20	1.154
30	0.612
40	0.866
50	0.841
60	0.938
70	0.654
80	0.671

TABLE II. The energy eigenvalues calculated with the single-particle model potential of Ref. 6, for the core charges $Z_C = 10$, 20, 30, and 40. The values of Z_I are chosen for all closed subshells. The energies E_{nl} are given in rydbergs.

Z_C	Z_I	1s	2s	2p	3s	3p	3d	4s	4p
10	8	98.02							
	6	91.45	18.50						
	0	64.20	3.38	1.88					
20	18	398.0							
	16	391.4	92.84						
	10	362.0	72.25	70.70					
	8	350.4	64.64	62.51	20.88				
	2	311.4	40.79	36.80	7.70	6.58			
30	28	898.0							
	26	891.0	216.6						
	20	859.8	191.7	190.7					
	18	847.2	182.3	180.7	68.10				
	12	804.9	151.8	148.4	48.15	46.59			
	2	723.1	96.9	89.7	15.65	13.38	7.60		
40	38	1598							
	36	1591	391.3						
	30	1559	365.2	364.6					
	28	1547	355.1	354.0	142.8				
	22	1503	322.1	319.2	119.5	17.2			
	12	1419	261.1	254.5	79.0	76.0	70.0		
	10	1401	248.2	240.8	70.8	67.6	60.0	25.7	
	4	1343	208.7	198.6	46.5	42.7	33.4	11.6	10.7

$$\Lambda_B^{l\pm}(r, r') = (1/\pi r r') \sin P u \,, \tag{2.3}$$

where

$$P(v) = [-2V(r) - L_\pm^2/v^2]^{1/2} \tag{2.4}$$

and

$$u = r - r' \,, \quad v = \tfrac{1}{2}(r + r') \,, \quad L_\pm^2 = (l_\pm + \tfrac{1}{2})^2 \,. \tag{2.5}$$

TABLE III. Same as Table II, for $Z_C = 50$ and 60.

Z_C	Z_I	1s	2s	2p	3s	3p	3d	4s	4p	4d	4f
50	48	2498									
	46	2491	616								
	40	2459	588	588							
	38	2446	578	577	239						
	32	2402	542	540	213	212					
	22	2315	476	480	166	164	156				
	20	2296	462	456	157	150	146	68			
	14	2237	419	410	128	124	113	49	48		
	4	2130	343	329	79	73	60	19	18	13	
60	58	3598									
	56	3591	890								
	50	3559	862	862							
	48	3545	851	851	359						
	42	3501	814	813	331	330					
	32	3413	745	740	280	277	270				
	30	3393	730	724	269	266	258	126			
	24	3333	683	676	237	233	222	104	102		
	14	3224	602	590	181	175	161	67	65	58	
	6	3131	534	518	136	129	111	39	37	29	19
	0	3057	481	462	102	95	74	19	18	10	

In (2.5), $l_\pm = l \pm 1$ are the angular momenta of the excited states reached by the dipole coupling from the initial state with the angular momentum l.

For a more general case in which the projection onto states which lie between E_a and E_b is desired, we have

$$\Lambda_{ab}^{l\pm}(r, r') = (1/\pi r r') (\sin P_b u - \sin P_a u) \,, \tag{2.6}$$

where

$$P_a(v) = [2E_a - 2V(v) - L_\pm^2 v^{-2}]^{1/2} \,,$$

$$P_b(v) = [2E_b - 2V(v) - L_\pm^2 v^{-2}]^{1/2} \,,$$

TABLE IV. Same as Table II, for $Z_C = 70$ and 80.

Z_C	Z_I	1s	2s	2p	3s	3p	3d	4s	4p	4d	4f	5s	5p	5d
70	68	4898												
	66	4891	1215											
	60	4858	1185	1186										
	58	4845	1174	1174	500									
	52	4799	1135	1134	470	469								
	42	4710	1061	1058	413	411	404							
	40	4690	1046	1041	401	399	391	195						
	34	4629	997	990	365	362	352	169	168					
	24	4518	910	899	303	298	283	126	124	116				
	10	4347	780	763	214	206	184	67	64	54	40			
	2	4242	703	681	162	153	127	35	33	22	8.7	5.8		
80	78	6398												
	76	6391	1589											
	70	6358	1559	1561										
	68	6344	1547	1549	665									
	62	6299	1508	1508	633	633								
	52	6209	1432	1429	574	572	566							
	50	6189	1416	1412	561	559	552	281						
	44	6127	1365	1360	523	520	510	253	252					
	34	6014	1275	1266	456	451	436	205	203	194				
	20	5841	1140	1124	359	351	329	138	135	123	107			
	12	5735	1059	1039	302	293	267	100	97	84	66	37		
	2	5597	954	929	231	220	189	54	51	38	19	10.1	10.0	

$E_a < E_b < 0$.

Note that, in the rescaled units of Appendix A,

$$P_a(\bar{v}) = \left(\frac{E_a}{4E_{nl}} - \frac{V(\bar{v})}{(E_{nl})^{1/2}} - \frac{L_\pm^2}{\bar{v}^2} \right)^{1/2} \tag{2.7}$$

with

$$\bar{v} = \tfrac{1}{2}(s+s'), \quad s \equiv 2(E_{nl})^{1/2} r \quad (E_{nl} > 0) .$$

In particular, we choose in the following $E_a = E_D$, $E_b = 0$, which gives $\Lambda_{ab}^{l\pm} \to \Lambda_D^{l\pm}$ for the projections onto states which lie between E_D and the ionization threshold.

For dipole coupling, the integrals of interest here are then given by

$$M_A^{nl\pm} = \langle nl | s^2 | nl \rangle , \tag{2.8}$$

$$M_B^{nl\pm} = \langle nl | \vec{s} \cdot \Lambda_B^{l\pm} \vec{s}' | nl \rangle , \tag{2.9}$$

$$M_C^{nl\pm} = M_A^{nl\pm} - M_B^{nl\pm} , \tag{2.10}$$

$$M_D^{nl\pm} = \langle nl | \vec{s} \cdot \Lambda_D^{l\pm} \vec{s}' | nl \rangle . \tag{2.11}$$

The values for E_D are chosen such that the transitions are only to the unoccupied levels of given $l_\pm = l \pm 1$, in accordance with the exclusion principle. Therefore, M_D corresponds to the correct transition probability to all the unoccupied bound states of the ion with Z_C and Z_I, while M_B includes transitions to *all* bound levels, some of which are forbidden by the exclusion principle. Throughout the calculation, we have taken E_D to be the $E_{nl_\pm}$ corresponding to the last-filled-subshell energies. Table V contains a sample for $Z_C = 20$.

TABLE V. The transition probabilities and overlap integrals for $Z_C = 20$, and in the dipole approximation. All values are given in atomic units. Z_I denotes the degree of ionization.

Z_I	nl	$l_\pm$	S	M_A	M_B	M_C	M_D
18	10	1	0.922	0.008	0.006	0.002	0.006
16	10	1	0.920	0.008	0.006	0.002	0.006
	20	1	0.960	0.107	0.104	0.003	0.104
10	10	1	0.914	0.008	0.005	0.002	0.001
	20	1	0.952	0.116	0.112	0.005	0.095
	21	0	0.960	0.085	0.085	0.000	0.044
	21	2	0.960	0.085	0.070	0.015	0.070
8	10	1	0.912	0.008	0.005	0.002	0.001
	20	1	0.949	0.121	0.115	0.006	0.098
	21	0	0.958	0.089	0.089	0.000	0.002
	21	2	0.958	0.089	0.071	0.018	0.071
	30	1	0.962	0.731	0.720	0.010	0.719
2	10	1	0.902	0.008	0.005	0.003	0.000
	20	1	0.929	0.142	0.130	0.012	0.008
	21	0	0.943	0.110	0.110	0.000	0.002
	21	2	0.943	0.110	0.068	0.042	0.068
	30	1	0.936	1.164	1.114	0.050	0.765
	31	0	0.955	1.149	1.151	0.002	0.724
	31	2	0.955	1.149	1.024	0.126	1.024

The accuracy of the projection operators Λ_B and Λ_D is partly reflected in the integral

$$S_{nl} = \langle nl | \Lambda_B^l | nl \rangle , \tag{2.12}$$

which should be unity if Λ_B^l were exact and the state $|nl\rangle$ is contained in Λ_B^l. This value is also given in Table V. We refer the readers to Ref. 7 where the accuracy of Λ_B^l was studied in detail for several cases where exact results are available for comparison. Except when M_B or M_C are very small compared with M_A, we expect our result to be fairly reliable.

Relativistic corrections are expected to be significant for K-shell electrons when $Z_C \gtrsim 50$. Because these inner electrons contribute little to the ionization processes when $Z_C > 40$ [see Fig. 2], we have ignored relativistic corrections to the atomic structure. The projectile electrons will be treated relativistically, however, in our final results.

Finally, it is of interest to compare the transition probabilities to the continuum calculated here with those for an hydrogenic atom given in Ref. 8. For this purpose, we write

$$\bar{c}_{nl} = \left(\frac{(l+1) M_C^{nl+} + l M_C^{nl-}}{2l+1} \right) \frac{E_{nl}}{3} , \tag{2.13}$$

where the factor $\frac{1}{3}$ is the average of the orientation of the dipole operators in (2.8)–(2.10). Table VI contains the result for $Z_C = 10$ and $Z_C = 60$, with $Z_I = 0$. Figure 1 also contains the result for $Z_C = 30$.

III. TOTAL IONIZATION CROSS SECTIONS

We consider the collision of a fast electron of momentum k_0 (energy $\epsilon_0 = k_0^2/2m$ large compared with single-orbital ionization energies) with an ion characterized by the charge parameters (Z_C, Z_I). The collision leads to a single-orbital transition $\alpha \to \beta$, where $\alpha = n, l$, etc. The final momentum of the impacting electron is k_β, where

$$\epsilon_\beta = k_\beta^2/2m = \epsilon_0 - \Delta_{\alpha\beta} , \quad \Delta_{\alpha\beta} = E_\beta - E_\alpha . \tag{3.1}$$

Neglecting exchange terms involving the impacting electron, we may write the differential cross section in the form given by Mott and Massey[8]

$$I_{\alpha\beta}(\theta) = \left(\frac{m}{2\pi} \right)^2 \frac{k_\beta}{k_0} Z_\alpha \times \left| \iint d^3r\, d^3r_0\, \phi_\beta^*(r)\, V_s\, \phi_\alpha(r)\, e^{i\vec{q}\cdot\vec{r}_0} \right|^2 , \tag{3.2}$$

where the ϕ's are single-electron orbital states,

$$\vec{q} = \vec{k}_0 - \vec{k}_\beta = q\hat{n} , \tag{3.3}$$

θ is the scattering angle, and

$$V_s = e^2/|\vec{r}_0 - \vec{r}| . \tag{3.4}$$

We take Z_α to be the number of electrons in the

shell $\alpha = (n, t)$.

For high-energy impacts, we may use the dipole approximation[8]

$$\int d^3r_0\, e^{i\vec{q}\cdot\vec{r}_0}\, V_s = (4\pi e^2/q^2)\, e^{i\vec{q}\cdot\vec{r}}$$

$$\approx (4\pi e^2/q^2)\,(1 + iq\,\vec{r}\cdot\hat{n}) \qquad (3.5)$$

Thus,

$$I_{\alpha\beta}(\theta) = 8\pi\,(k_\beta/k_0\,q^2)\,Z_\alpha\,M_{\alpha\beta}\,, \qquad (3.6)$$

where

$$M_{\alpha\beta} = \left|\int d^3r\,\phi_\beta^*(r)\,\phi_\alpha(r)\,\vec{r}\cdot\vec{n}\right|^2/a_0^2\,. \qquad (3.7)$$

Now,

$$k_0\,k_\beta \sin\theta\, d\theta = q\, dq \cong k_0^2 \sin\theta\, d\theta\,, \qquad (3.8)$$

so we may introduce

$$J_{\alpha\beta}(q)\, dq = 2\pi I_{\alpha\beta}(\theta)\, k_\alpha\, k_\beta \sin\theta\, d\theta/q\,, \qquad (3.9)$$

or the total cross section

$$\sigma_{\alpha\beta}(k_\alpha) = \int_{q_{\min}}^{q_{\max}} J_{\alpha\beta}(q)\, dq$$

$$\approx (4\pi Z_\alpha/k_0^2)\, M_{\alpha\beta} \ln(4\epsilon_0/\Delta_{\alpha\beta})\,. \qquad (3.10)$$

Here, we have used high-energy nonrelativistic kinematics[9] to determine the limits on q as

$$q_{\min} \approx m\,\Delta_{\alpha\beta}/k_\alpha\,, \quad q_{\max} \approx (2mE_0)^{1/2}\,. \qquad (3.11)$$

We consider first the direct ionization to continuum states. When the expression (3.9) for $\sigma_{\alpha\beta}$ is summed over all available final states, we have

$$\sigma_\alpha^C(k_\alpha) = \sum_\beta^C \sigma_{\alpha\beta}^C \approx \sum_\beta^C \frac{4\pi Z_\alpha}{k_\alpha^2}\, M_{\alpha\beta}^C \ln\left(\frac{4\epsilon_\alpha}{\Delta_{\alpha\beta}^C}\right)$$

$$\equiv \frac{4\pi Z_\alpha}{k_\alpha^2} \ln\left(\frac{4\epsilon_\alpha}{\Delta_\alpha^C}\right) M_C^\alpha\,, \qquad (3.12)$$

where

$$M_C^\alpha = \sum_\beta^C M_{\alpha\beta}^C\,, \quad \alpha = (n, l)\,, \qquad (3.13)$$

TABLE VI. Comparison of the transition probabilities to the continuum as calculated here and those given in Ref. 8. $\bar{c}_{nl}$ is defined by (2.13).

Z_C	Z_I	nl	c_{nl}	$\bar{c}_{nl}$
10	0	10	0.28	0.36
		20	0.21	0.30
		21	0.13	0.20
60	0	10	0.28	0.30
		20	0.21	0.14
		21	0.13	0.32
		30	0.17	0.14
		31	0.14	0.20
		32	0.07	0.27
		40	0.15	0.18
		41	0.13	0.22
		42	0.09	0.54

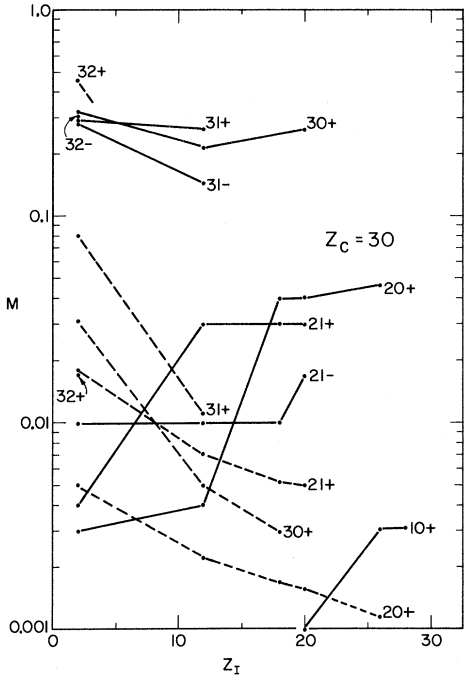

FIG. 1. Transition probabilities M_D to all the allowed bound states and M_C to all the continuum, at $Z_C = 30$. The numbers next to each curve are $nl+$ or $nl-$. The solid lines are the M_D values, while the dotted lines are for M_C.

and Δ_α^C is the average excitation energy defined by (3.12). Since both M_C^{nl+} and M_C^{nl-} are involved in our case, we replace M_C^α in (3.12) by its average

$$\bar{M}_C^{nl} \equiv \frac{1}{3(2l+1)}\,[(l+1)\,M_C^{nl+} + l\,M_C^{nl-}] \equiv \bar{M}_C^\alpha \qquad (3.14)$$

and set

$$Z_\alpha \equiv Z_{nl} = 2(2l+1) \qquad (3.15)$$

for each closed subshell. Thus, combining (3.12)–(3.15), we finally have (NR denotes nonrelativistic)

$$\sigma_\alpha^C(k_\alpha) = \pi a_0^2\, \frac{4Z_\alpha}{(k_0\,a_0)^2} \ln\left(\frac{4\epsilon_\alpha}{\Delta_\alpha^C}\right) \bar{M}_C^\alpha \ \text{(NR)}\,, \qquad (3.16)$$

and thus

$$\sigma^C(Z_C, Z_I, E) = \textstyle\sum_\alpha \sigma_\alpha^C\,. \qquad (3.17)$$

As discussed earlier, the ionization of the target ions is also possible through the excitation of an inner-shell electron followed by an Auger transition. This is then related to the transition matrix elements $M_D^{nl\pm}$ to all the allowed bound-state levels and also to the fluorescence yield. If we denote by W_α the probability that an Auger transition will follow excitation from the orbital state α, the cross section for ionization following collisional excitation is

$$\sigma_\alpha^A(k_\alpha)=\pi a_0^2\,\frac{4Z_\alpha}{(k_\alpha a_0)^2}\,\ln\!\left(\frac{4\epsilon_\alpha}{\Delta_\alpha^B}\right)\bar{M}_D^\alpha W_\alpha \quad \text{(NR)}\,, \tag{3.18}$$

which follows from the argument similar to that was used to obtain (3.16), and thus

$$\sigma^A(Z_C, Z_I, E)=\sum_\alpha \sigma_\alpha^A\,. \tag{3.19}$$

In (3.18), the W_α are given by the fluorescence yield Y_α as $W_\alpha = 1 - Y_\alpha$, and the actual values used in our calculation are given in Fig. 2, with $W_\alpha = 1$ for $n \geq 3$; Δ_α^B is the average excitation energy of the αth subshell, and

$$\bar{M}_D^\alpha=\frac{1}{3(2l+1)}\,[(l+1)M_D^{nl+}+lM_D^{nl-}]\,. \tag{3.20}$$

The total ionization cross section is finally given by

$$\sigma^I(Z_C, Z_I, E)=\sum_\alpha(\sigma_\alpha^C+\sigma_\alpha^A) \tag{3.21}$$

for each set of parameters Z_C, Z_I, and E.

In actual calculation, we simply used

$$\Delta_\alpha^C \approx \Delta_\alpha^B \approx E_I\,, \tag{3.22}$$

where E_I is the ionization potential for the electron in the highest-filled subshell. Since the cross sections depend on Δ only logarithmically, the choice (3.22) is not expected to affect the result drastically. An improved treatment of the ln factor is possible, however, and this is outlined in Appendix B, where a procedure to estimate the average excitation energy is presented.

When the incident electron is relativistic, we have to modify (3.16) and (3.18) slightly as[8]

$$\ln(4\epsilon_\alpha/\Delta_\alpha) \to \ln(4\epsilon_\alpha\gamma/\Delta_\alpha)-\beta^2 \tag{3.23}$$

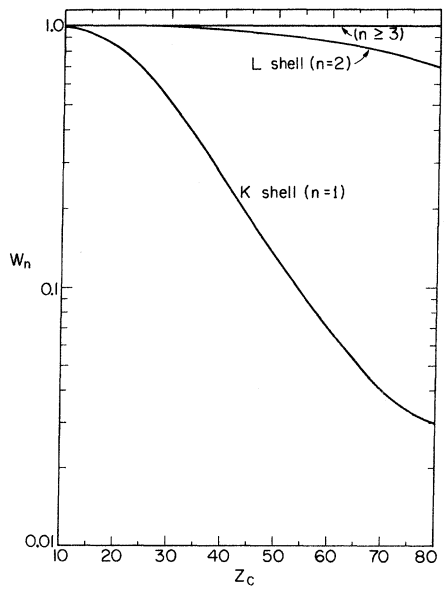

FIG. 2. Relative Auger branching ratio as estimated from the fluorescence yield calculations.

and

$$k_\alpha a_0 \to \beta/\alpha_0\,, \tag{3.24}$$

where

$$\alpha_0=e^2/\hbar c=\tfrac{1}{137}\,, \quad \gamma=(1-\beta^2)^{-1/2}\,, \quad \beta=v/c\,.$$

Thus, we have explicitly, at high energies with relativistic electron beams and with $E=\gamma mc^2$ (ER denotes extreme relativistic),

$$\sigma_\alpha^C=\pi a_0^2\,\frac{4\alpha_0^2}{\beta^2}\left[\ln\!\left(\frac{2\beta^2E}{\Delta_\alpha^C}\right)-\beta^2\right]Z_\alpha\bar{M}_C^\alpha \quad \text{(ER)}\,, \tag{3.25}$$

$$\sigma_\alpha^A=\pi a_0^2\,\frac{4\alpha_0^2}{\beta^2}\left[\ln\!\left(\frac{2\beta^2E}{\Delta_\alpha^B}\right)-\beta^2\right]Z_\alpha\bar{M}_D^\alpha W_\alpha \quad \text{(ER)}\,. \tag{3.26}$$

In Table VII, both NR forms (3.16), (3.18), and the ER forms (3.25), (3.26) of cross sections are used to calculate the total ionizations. The result at $\epsilon_0 = 1$ and at 10 keV seems to agree reasonably well with the earlier calculations and also with the experimental value. We note that the contribution of σ^A is not negligible.

Individual values of σ^C and σ^A for various Z_C and $Z \equiv Z_C - Z_I$ are presented in Fig. 3. For given Z, σ^C seems to dominate at small Z_C, but this trend is reversed for large Z_C, with σ^A dominating at high Z_C. The total ionization cross section σ^I is given in Fig. 4 for an electron energy of 20 MeV. The cross section at other energies may be scaled from Fig. 4 and Eqs. (3.10), (3.18), (3.25), and (3.26).

IV. DISCUSSION

The ionization cross sections that we have obtained in Sec. III are based on a rather crude model for the electron orbital states. The comparisons in Tables VI and VII with the corresponding exact calculations given in Ref. 8 (for hydrogen, however, so that direct comparison is not possible) and with some experimental cross sections provide an indication of the accuracy of our cross sections. We have made several of the "standard" high-energy approximations and these of course limit the energy range over which our expressions can be used.

The previous estimates[3] of σ^I do not include the contribution of σ^A, which requires both $\bar{M}_D^\alpha$ and W_α. Since σ^A seems to dominate the ionization cross sections at high Z_C, any agreement previously existing between the theoretical calculations and experiments could be fortuitous.

ACKNOWLEDGMENTS

We would like to thank Dr. M. Rotenberg and Dr. F. Gilmore for some of the recent references on the Thomas–Fermi model and Auger-transition calculations, and also Dr. Hans Mark for sending us a preprint of a forthcoming review of Auger pro-

cesses and fluorescent yields. The present calculation has been carried out at the request of Dr. L. J. Laslett and the E. R. A. group. One of us (Y. H.) would like to thank the members of the Physics Department at Lawrence Berkeley Laboratory for their hospitality.

APPENDIX A

The calculation of the eigenvalues and eigenfunctions with the local potential $V(r)$ given in Sec. II is well known, but we briefly describe the procedure used in our calculation so that results at other values of Z_C and Z_I than those presented here could be readily reproduced.

The single-particle energies and wave functions are calculated in the usual way by solving the radial equation

$$\left(-\frac{d^2}{dr^2}+\frac{l(l+1)}{r^2}+2V(r)+E_{nl}\right)R_{nl}(r)=0\ , \qquad \text{(A1)}$$

where E_{nl} is given in Rydberg units. Since a large variation in Z_C and E_{nl} is involved, we rescale the variable r such that (A1) becomes

$$\left(-\frac{d^2}{ds^2}+\frac{2V(s)}{2(E_{nl})^{1/2}}+\frac{1}{4}+\frac{(l+\frac{1}{2})^2-\frac{1}{4}}{s^2}\right)R_{nl}(s)=0\ , \qquad \text{(A2)}$$

with

$$s=2(E_{nl})^{1/2}r \quad (E_{nl}>0)\ ,$$

$$V(s)=V(r\to s,\ d\to d'=2(E_{nl})^{1/2}d)\ .$$

The solutions obtained by integrating (A2) in from the large values of s and out from $s\approx 0$ are matched at $s=s_0$, $s_0\approx 20h$ with $h=0.2$ in the above unit.

The starting values for the integrations are calculated as follows.

a. $s=0$ region. Using the expansion of the regular Whittaker function,[10]

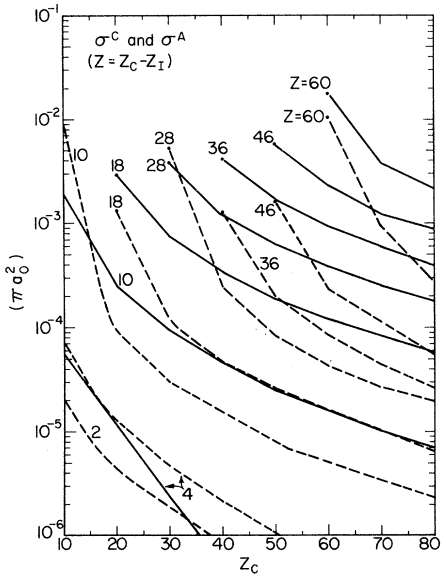

FIG. 3. Estimated ionization cross sections σ^C and σ^A corresponding to the direct excitations to the continuum and the excitations to bound states followed by the Auger emissions, respectively. $Z=Z_C-Z_I$, where Z_C is the core charge and Z_I is the degree of ionization of the target before the collision. All values are given in πa_0^2 units and the electron energy is 20 MeV. The solid lines are the values for σ^A, while the dotted lines are for σ^C.

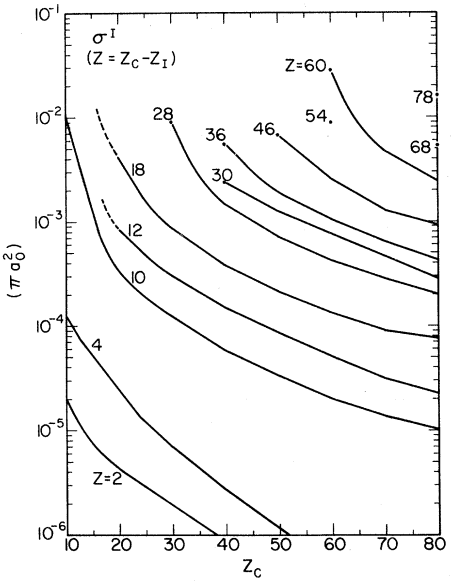

FIG. 4. Total ionization cross sections for 20-MeV electrons as functions of Z_C and $Z=Z_C-Z_I$. All values are given in πa_0^2 units.

TABLE VII. The ionization cross sections σ^C, σ^A, and σ^I in units of πa_0^2, where a_0 = Bohr radius. σ^B corresponds to total excitation cross section to all the bound states, where the effect of the exclusion principle is neglected. The experimental values are summarized in Ref. 3; $Z_C=10$, $Z_I=0$, $Z=Z_C-Z_I=10$.

$\epsilon_0=1$ keV:	$\sigma^B=0.363$	
	$\sigma^C=0.396$	
	$\sigma^A=0.087$	
	$\sigma^I=0.483$	Expt. $\sigma^I\approx 0.35\sim 0.43$
$\epsilon_0=10$ keV:	$\sigma^B=0.053$	
	$\sigma^C=0.058$	
	$\sigma^A=0.013$	
	$\sigma^I=0.071$	Expt. $\sigma^I\approx 0.07$
$E=20$ MeV:	$\sigma^B=0.0049$	
	$\sigma^C=0.0083$	
	$\sigma^A=0.0019$	
	$\sigma^I=0.0102$	

$$R_{nl}(s)\approx M_{km}(s)=s^{1/2+m}e^{-s/2}\left(1+\frac{\frac{1}{2}+m-k}{1!(2m+1)}\,s\right.$$
$$\left.+\frac{(\frac{1}{2}+m-k)(\frac{3}{2}+m-k)}{2!(2m+1)(2m+2)}\,s^2+\cdots\right), \quad \text{(A3)}$$

where

$$k=Z_C/(E_{nl})^{1/2}, \qquad m=\tfrac{1}{2}\ .$$

That is, the dominant part of $V(r)$ near $r=0$ is taken to be purely Coulombic with the charge Z_C. The correction to the wave function coming from the non-Coulombic part of $V(s)$ is then included by integrating out with the finer mesh size $h'=0.1h$. In this way, the starting values of R_{nl} and R'_{nl} at $s=h$ for further integration outward with $\Delta s=h$ are generated.

b. s large. Since the core charge Z_C is in general screened by the Z_C-Z_I-1 electrons, we have to modify the value of k in the region of large s, as

$$k\to\kappa=(Z_I+1)/(E_{nl})^{1/2}, \qquad m=\tfrac{1}{2}\ .$$

Thus, we have[10]

$$R_{nl}\approx W_{\kappa m}(s)=e^{s/2}s^{\kappa}\left(1+\frac{m^2-(\kappa-\frac{1}{2})^2}{1!s}\right.$$
$$\left.+\frac{[m^2-(\kappa-\frac{1}{2})^2][m^2-(\kappa-\frac{3}{2})^2]}{2!\,s^2}+\cdots\right). \quad \text{(A4)}$$

Typically, the starting values are evaluated at $s\approx 27$ in the rescaled atomic units.

c. Matching of logarithmic derivatives made at $s=s_0=20h$, $h=0.2$, except when they are very small in this region. The value of $E_{nl}^{(t)}$ guessed initially is corrected by the formula

$$E_{nl}\approx E_{nl}^{(t)}+\Delta_{nl}\ ,$$

where

$$\Delta_{nl}=\left(\int_0^{s_0}\frac{u_t^2\,ds}{(u_t^2|_{s=s_0})}+\int_{s_0}^{\infty}\frac{v_t^2\,ds}{(v_t^2|_{s=s_0})}\right)$$
$$\times\left(\frac{v_t'}{v_t}-\frac{u_t'}{u_t}\right)^{-1}_{s=s_0}. \quad \text{(A5)}$$

In (A5), u_t and v_t are the functions obtained by integrating out and in, respectively. With a reasonable initial guess on $E_{nl}^{(t)}$, the procedure converged within five integrations to an accuracy of one part in 10^4. Note that the variable r is rescaled as E_{nl} is changed.

In view of the crudeness of the model used, the eigenvalues E_{nl} are not expected to be very accurate, especially for the higher excited states. In fact, the variations among the values obtained with different models are substantial. Therefore, R_{nl} and E_{nl} are calculated here only to the accuracy which is sufficient to give a rough estimate of the excited states involved.

APPENDIX B

The average excitation energies Δ_α^B and Δ_α^C introduced in Sec. III may be estimated more accurately if we write, by definition,

$$M_B^{(\alpha)}\ln\left(\frac{4\epsilon_\alpha}{\Delta_\alpha^B}\right)\equiv\sum_\beta{}^{B\,\prime}\,|\langle\alpha|\vec{r}_1\cdot\vec{n}|\beta\rangle|^2\ln\left(\frac{4\epsilon_\alpha}{E_\alpha-E_\beta}\right), \quad \text{(B1)}$$

and similarly for Δ_α^C where $M_C^{(\alpha)}$ is given by (3.13). The range of the β sum is such that

$$0<E_\alpha-E_D<\Delta_\alpha^B<E_D\ , \qquad E_\alpha<\Delta_\alpha^C<\infty\ . \quad \text{(B2)}$$

The right-hand side of (B1) may be evaluated using the identity

$$\ln\left(\frac{4\epsilon_\alpha}{E_\alpha-E_\beta}\right)=\ln\left(\frac{4\epsilon_\alpha}{E_\alpha}\right)+\ln\left(\frac{E_\alpha}{E_\alpha-E_\beta}\right)$$
$$=\ln\left(\frac{4\epsilon_\alpha}{E_\alpha}\right)+\int_0^1 dc\left\langle\beta\left|\frac{D}{E_\alpha-cD}\right|\beta\right\rangle \quad \text{(B3)}$$

where the operator D is defined such that

$$D|\beta\rangle=F_\beta|\beta\rangle \quad (E_\beta>0 \text{ for bound states}),$$
$$[D,\Lambda_\beta]=0=[D,\Lambda_C]\ . \quad \text{(B4)}$$

Therefore, (B1) may be rewritten as

$$\ln(4\epsilon_\alpha/\Delta_\alpha^\beta)$$
$$=(1/M_\beta^{(\alpha)})\left[\langle\alpha|\vec{r}_1\cdot\vec{n}\,\Lambda_\beta\,\vec{r}_1'\cdot\vec{n}|\alpha\rangle\ln(4\epsilon_\alpha/E_\alpha)\right.$$
$$\left.+\int_0^1 dc\,\langle\alpha|\vec{r}_1\cdot\vec{n}\,\tilde{G}_\alpha^B D\,\vec{r}_1'\cdot\vec{n}|\alpha\rangle\right]\ , \quad \text{(B5)}$$

where

$$\tilde{G}_\alpha^B\equiv\left(\frac{1}{E_\alpha-cD}\right)_B\ . \quad \text{(B6)}$$

As in Secs. II and III, we may now replace the Λ_B and $\tilde{G}_\alpha^B$ by their semiclassical approximations. That is,[7]

$$\Lambda_B\to\frac{1}{2\pi^2 u}\sin P(v)u \quad \text{(B7)}$$

and

$$\tilde{G}_\alpha^B\to\frac{1}{\pi^2 u}\int_0^{P(v)}\frac{p\,dp\,\sin pu}{2E_\alpha-cp^2-2cV(v)}\ , \quad \text{(B8)}$$

where $V(v)$ is the single-particle model potential defined in Sec. II. Similar expressions can be derived for Δ_α^C by replacing in (B5) the subspace label B by C.

We do not consider (B5) further in this paper, since Δ_α^B and Δ_α^C appear in the cross sections only logarithmically so that their effect would not be expected to change the over-all estimate of σ in any serious way.

*Research supported in part by the U. S. Atomic Energy Commission and by the Air Force Office of Scientific Research, Office of Aerospace Research, United States Air Force, under Contract No. F44620-70-C-0028.

†On sabbatical leave from the Physics Department, University of Connecticut, Storrs, Conn. 06268. Participating guest, Lawrence Berkeley Laboratory.

[1]See E. J. McGuire [Phys. Rev. A 5, 1052 (1972); 3, 587 (1971)], where many of the earlier references could be found. Also W. Fink, R. C. Jopson, H. Marks, and C. D. Swift, Rev. Mod. Phys. 38, 513 (1966); W. Bambynek, B. Crasemann, F. W. Funk, H. U. Freund, H. Mark, C. D. Swift, R. E. Price, and P. V. Rao, Rev. Mod. Phys. 44, 716 (1972).

[2]V. O. Kostroun, M. H. Chen, and B. Crasemann, Phys. Rev. A 3, 533 (1971); 4, 1 (1971).

[3]See, for example, K. Omidvar, H. L. Kyle, and E. C. Sullivan, Phys. Rev. A 5, 1174 (1972).

[4]F. Herman and S. Skillman, *Atomic Structure Calculations* (Prentice-Hall, Englewood Cliffs, N. J., 1963).

[5]For example, R. Latter, Phys. Rev. 99, 510 (1955); J. C. Stewart and M. Rotenberg, *ibid.* 140, A1508 (1965).

[6]A. E. S. Green, D. L. Sellin, and A. S. Zachor, Phys. Rev. 184, 1 (1969).

[7]Y. Hahn and K. M. Watson, Phys. Rev. A 6, 548 (1972).

[8]N. F. Mott and H. S. W. Massey, *The Theory of Atomic Collisions* (Oxford U.P., Oxford, England, 1965), Chap. 16.

[9]Corrections for a relativistic impacting electron will be introduced later.

[10]E. T. Whittaker and G. N. Watson, *A Course of Modern Analysis* (Cambridge U.P., Cambridge, England, 1952), pp. 337–342.

PHYSICAL REVIEW A VOLUME 7, NUMBER 2 FEBRUARY 1973

Distorted-Wave Approximation and Its Application to the Differential and Integrated Cross Sections for Electron-Impact Excitation of the 2 ^1P State of Helium*

D. H. Madison and W. N. Shelton

Department of Physics, The Florida State University, Tallahassee, Florida 32306

(Received 15 December 1971; revised manuscript received 25 September 1972)

Theoretical results are given for the application of the distorted-wave approximation to electron-atom impact excitation for transitions from an L-S coupled initial state to an arbitrarily coupled final state. Expressions for the differential cross section and spin polarization of the emitted electrons are given for unpolarized electron beams incident upon unpolarized atoms. These results are applied to excitation of helium from its ground state to the $1s2p\ ^1P_1$ excited state for incident-electron energies between 26.5 and 300 eV. The results are compared with previous theoretical and experimental works. It is found that the distorted-wave calculation is superior to previous calculations in fitting the absolute magnitude and angular distribution of the experimental data. The improvement over the plane-wave calculations is greater at large angles, where the plane-wave approximations fail by several orders of magnitude.

I. INTRODUCTION

Until a few years ago, theories of electron-impact excitation were judged principally on their ability to predict integrated cross sections, while today there is an increasing emphasis on the correct prediction of the angular distributions as well. Recently there has also been an increasing interest in the spin polarization of the scattered electrons. This interest has been stimulated by the appearance of reliable experimental polarization data for unpolarized electron beams on unpolarized atomic targets. We can expect in the near future that theories of electron-impact excitation will be required to predict not only correct integrated and differential cross sections, but also correct angular distributions of electron spin polarization. It seems likely that those theories which predict incorrect spin polarization, or which yield no information of this type, can be expected to be of decreasing importance.

For the past several years many calculations have been made for inelastic electron-atom scattering cross sections using the Born[1,2] and other related plane-wave approximations.[3–10] These approximations give fairly good integrated cross sections, at high energy, for allowed transitions. The shape of the small-angle differential cross sections is reasonably good for allowed transitions provided the momentum transfer is small and the incident energy is sufficiently high.[8,11] However, the angular range over which the Born approximation gives approximately correct results decreases with increasing incident-electron energy. At a given incident-electron energy, the breakdown at large angles occurs rapidly once it has begun, so that an error of many orders of magnitude is quite common. As for the plane-wave exchange approximations, there is no evidence that any of them give even qualitatively correct angular distributions at